Fig. s1

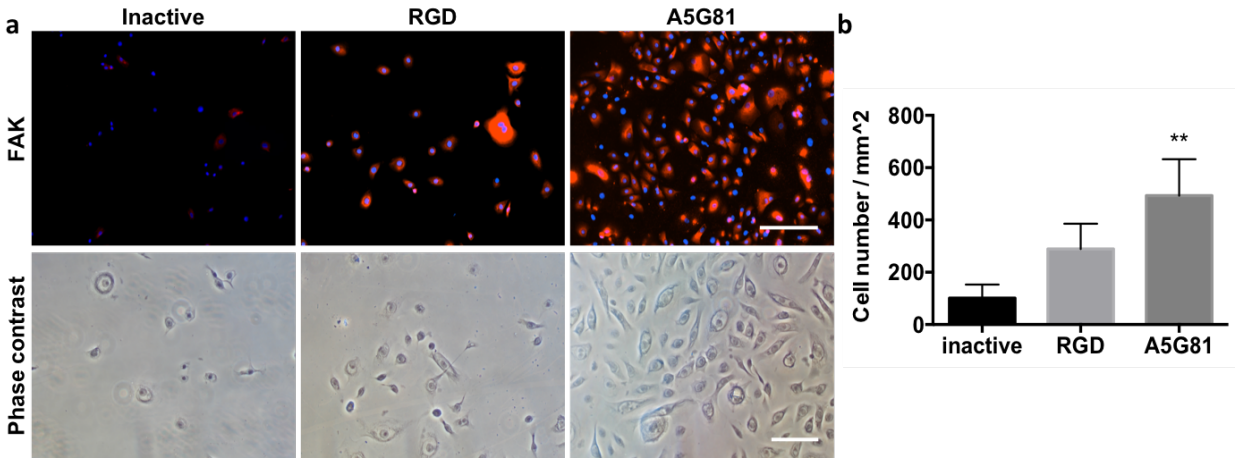

Figure s1 | A5G81 promotes the cell adhesion and focal adhesion kinase (FAK) expression on 2D SAM surfaces. Human primary HEKa cells were seeded at a concentration of 20,000/cm^2 and allowed to attach and develop focal adhesion to the peptide-presenting SAM surfaces. After 12 hours of incubation, the cell-seeded SAM surfaces were washed and probed with anti-FAK antibody. **(a)** Representative anti-FAK-fluorescence (top) and phase contrast (bottom) images of the adherent HEKa cells. The fluorescence and the phase contrast images correspond to cells at different locations within each sample type (scale bar: 100 μm); **(b)** cell adhesion was quantified based on the nuclei (DAPI, blue) staining (n=6, ** p< 0.01). The results indicate that the adhesion of HEKa and the expression of FAK were significantly enhanced on SAMs displaying the A5G81 peptide.

Fig. s2

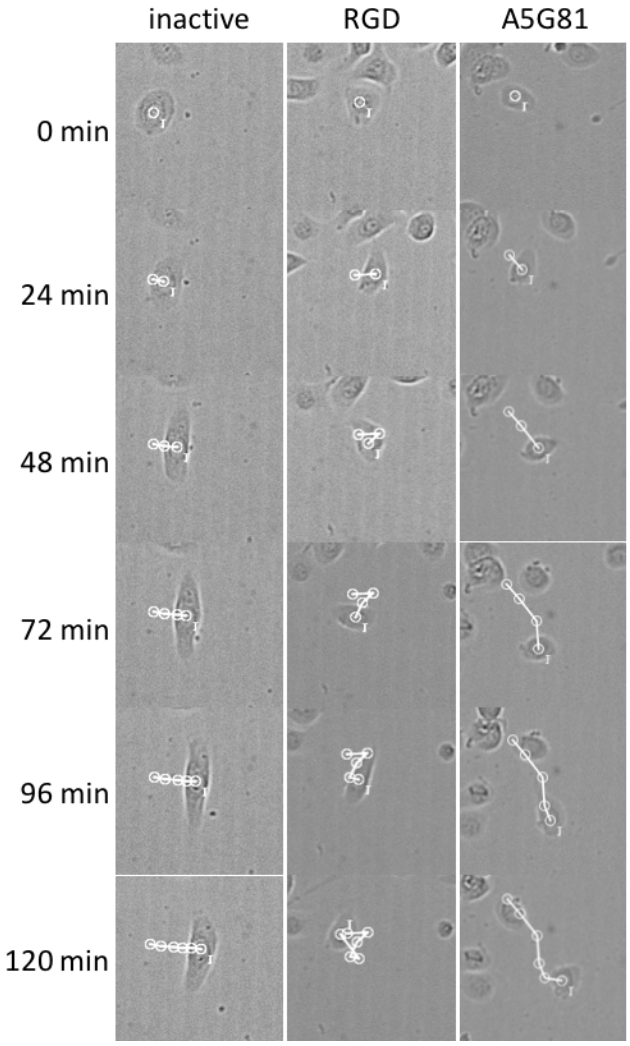

Figure s2 | A5G81 promotes HEKa migration via haptokinesis. Time-lapse microscopy showing the migration of HEKa on a self-assembled monolayer presenting the inactive, RGD or A5G81 peptides at a density of 1% against tri(ethylene glycol) groups. Images were collected at 20 min intervals. Images were analyzed using ImageJ to create trajectories for individual cells. The images are overlaid with open circles that track the position of the cell at each time interval.

Fig. s3

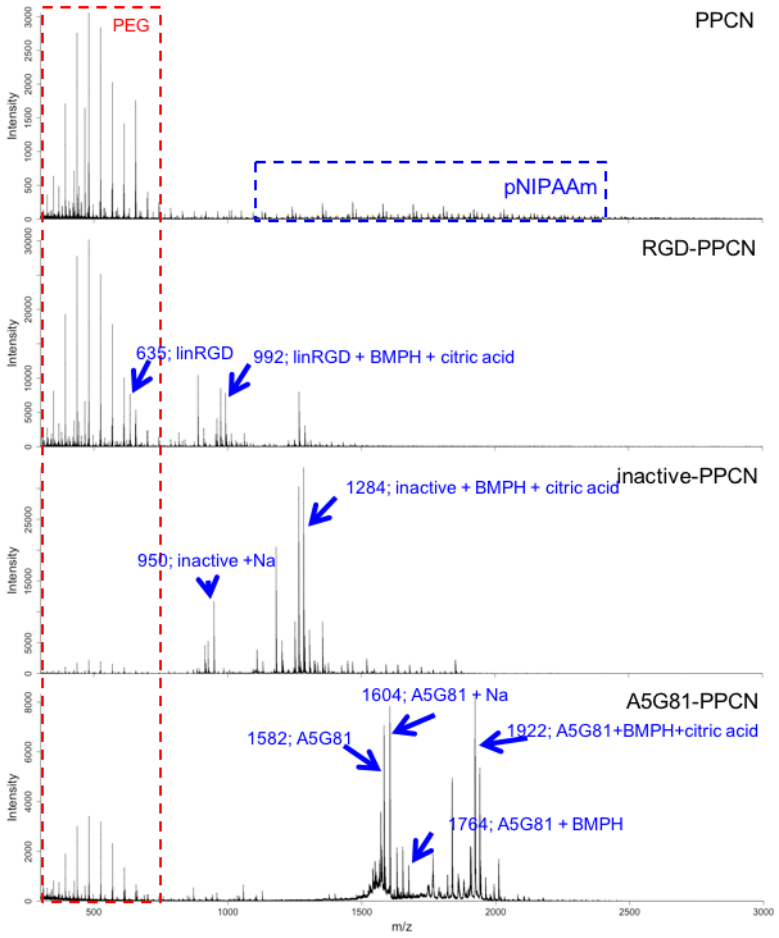

Figure s3 | MALDI-TOF characterization of the Peptide-PPCN. The presence of tethered peptides was detected through matrix-assisted laser desorption/ionization (MALDI) mass spectrometry. The spectra show the presence of the PPCN, peptide, peptide-linker, or peptide- linker-citric acid constructs, confirming the successful conjugation of the peptide to PPCN.

Fig. s4

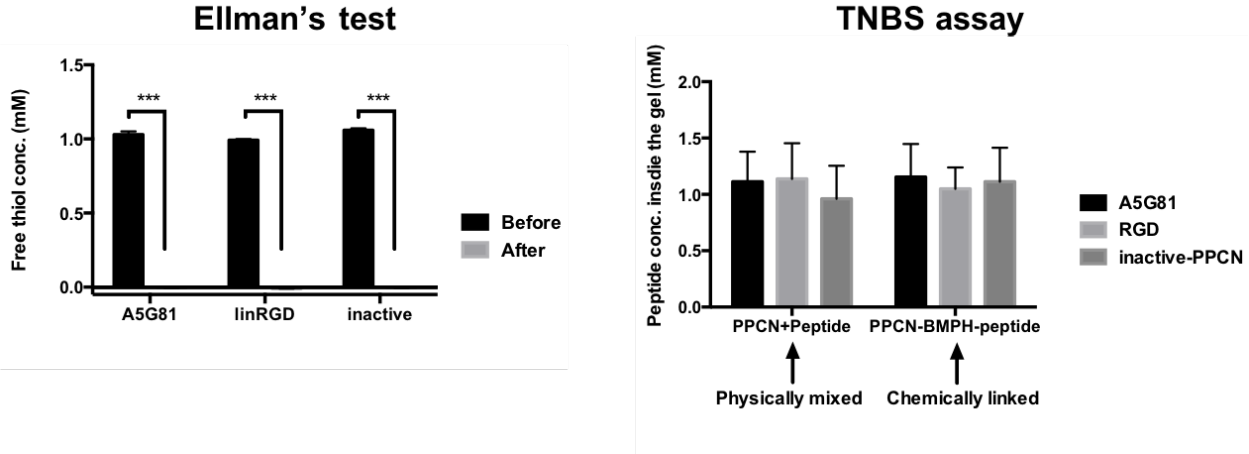

Figure s4 | Peptide molar concentration was the same (1mM) for all three groups of peptide-PPCN. In order to determine the final peptide concentration in the peptide-modified PPCN: **(a)** Ellman's test was conducted to measure the unreacted free peptide concentration in the solution before and after conjugation. The free peptide concentration in the solution after the reaction time was approximately 0, demonstrating the complete conjugation of 1 mM peptides in all three groups, **(b)** Primary amines assessed via the TNBS assay were used to directly measure the final concentration of peptide tethered to the PPCN, which was approximately 1 mM for all three groups of hydrogels. Known concentrations of free peptides mixed with PPCN (no maleimide) were used as a reference to validate the results (n=5, *** $p < 0.001$)

Fig. s5

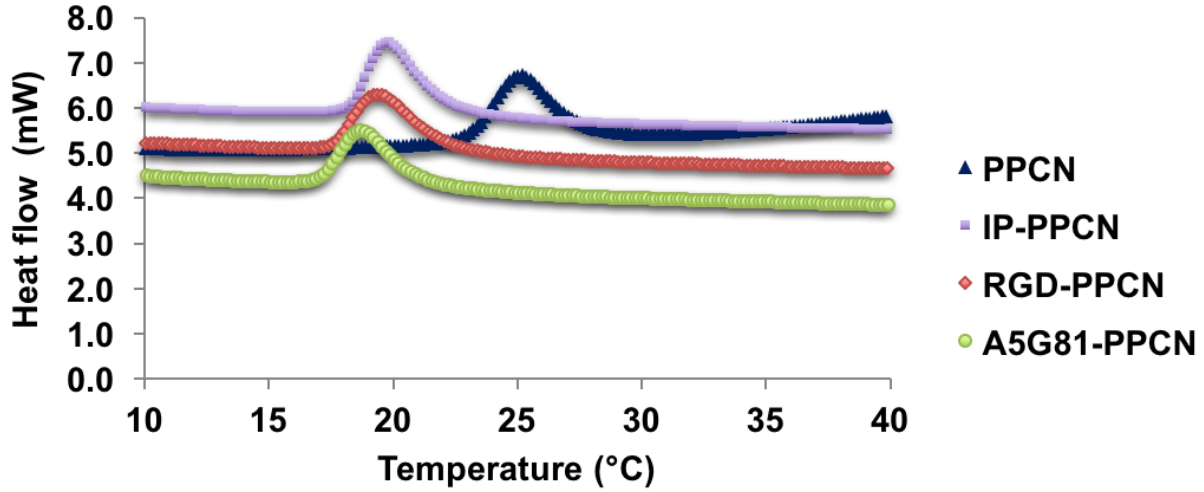

Figure s5 | Transition temperature characterization of the Peptide-PPCN with differential scanning calorimetry (DSC). Heat flow determination of the gelation temperature of the various hydrogels.

Figure s6

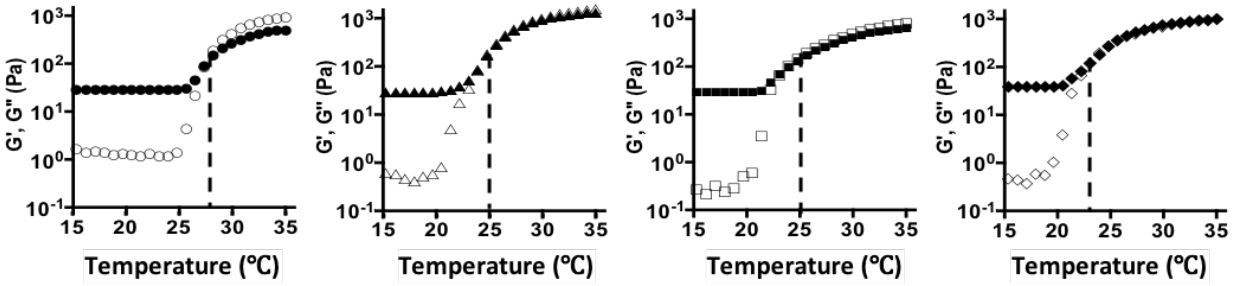

	PPCN	
Temperature	G'	G"
15.325	1.59243	27.5268
16.242	1.33979	27.2259
17.123	1.4658	27.7963
17.975	1.37272	27.604
18.838	1.24346	27.7784
19.69	1.29764	27.6756
20.544	1.22245	27.9213
21.381	1.14571	27.7607
22.244	1.2666	27.8441
23.121	1.15959	28.1114
23.962	1.15488	27.6203
24.803	1.3287	28.1255
25.679	4.21032	29.8852
26.532	21.0944	43.7717
27.379	82.1858	88.8468
28.243	182.079	144.889
29.122	299.726	203.251
29.93	417.799	258.351
30.834	541.258	315.433
31.677	647.576	364.688
32.522	742.781	408.945
33.396	816.643	443.936
34.22	871.797	472.717
35.08	908.655	493.77

	inactive-PPCN	
Temperature	G'	G''
15.291	0.617058	30.0078
16.227	0.591605	30.0688
17.099	0.463994	30.0357
17.969	0.430406	29.9455
18.806	0.536599	30.2576
19.691	0.607096	29.9138
20.51	0.840755	30.4866
21.376	5.1799	32.2767
22.217	17.5395	39.1096
23.104	35.6836	51.2375
23.942	82.3986	89.1089
24.817	180.477	176.85
25.684	303.932	291.204
26.535	441.61	420.011
27.342	587.373	555.841
28.246	738.302	696.125
29.088	880.776	825.683
29.927	1014.32	943.449
30.815	1137.25	1048.72
31.649	1246.35	1136.56
32.53	1341.66	1208.85
33.361	1420.59	1262.89
34.205	1486.43	1303.49
35.036	1537.54	1329.9

	RGD-PPCN	
Temperature	G'	G"
15.289	0.264699	29.4268
16.213	0.213821	29.3764
17.078	0.312864	29.3754
17.954	0.23788	29.5373
18.814	0.275595	29.4779
19.694	0.507324	29.3434
20.521	0.596708	29.7259
21.391	3.35756	30.7782
22.251	31.1375	47.1516
23.098	63.5885	67.5464
23.951	101.874	95.0131
24.806	145.736	131.195
25.668	189.742	170.701
26.509	237.299	214.172
27.347	289.743	262.011
28.234	347.542	313.346
29.072	407.001	364.486
29.942	467.635	414.891
30.778	526.206	461.038
31.614	583.687	506.091
32.511	637.129	544.598
33.325	686.598	577.535
34.216	730.884	606.833
35.054	772.545	633.716

	A5G81-PPCN	
Temperature	G'	G"
15.347	0.450886	37.4157
16.248	0.431799	37.7931
17.093	0.358064	37.8293
17.964	0.58058	37.8993
18.801	0.537584	38
19.645	1.02731	38.1489
20.504	3.7584	39.0409
21.365	28.2336	55.521
22.248	66.1756	80.147
23.083	117.234	115.811
23.957	188.768	175.995
24.811	271.173	255.786
25.654	349.507	340.98
26.517	420.93	424.074
27.363	488.259	503.603
28.204	554.805	578.966
29.079	620.673	648.894
29.915	684.923	714.031
30.775	746.985	772.615
31.621	804.543	822.57
32.494	858.67	865.15
33.331	907.26	899.409
34.191	951.442	928.324
35.041	991.914	951.685

Figure s6 | Rheological determination of the lower critical solution temperature of the various hydrogels (black marker-loss modulus G”; white marker-storage modulus G’; Top left: PPCN, top right: inactive-PPCN, bottom left: RGD- PPCN, bottom right: A5G81-PPCN, Table: actual G’ and G” data for the peptide-PPCN).

Fig. s7

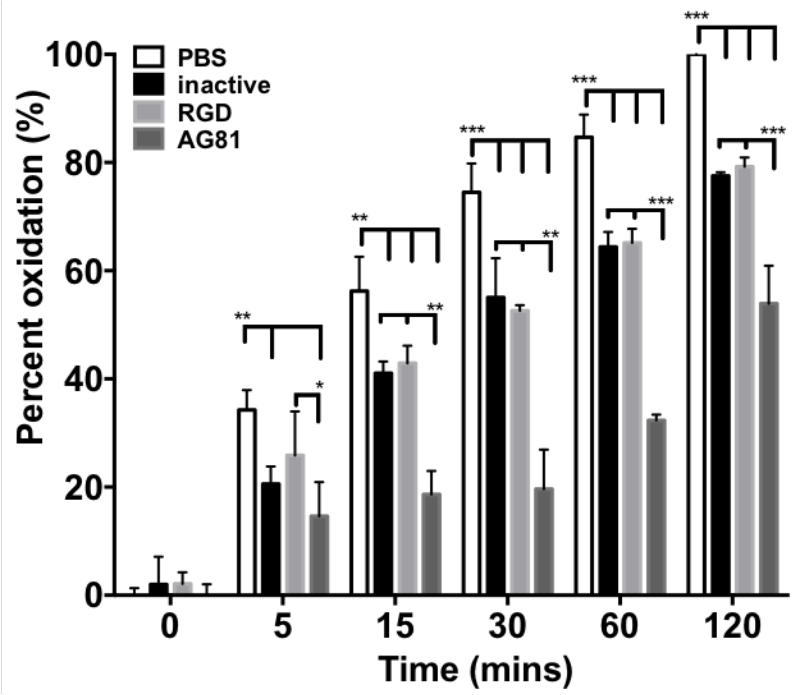

Figure s7 | β-carotene lipid peroxidation inhibition assay results demonstrate antioxidant activity of the peptides in solution. (n=6, * $p < 0.05$; ** $p < 0.01$; *** $p < 0.001$)

Table. s1

	PPCN						inactive-PPCN					
	Day 5			Day 10			Day 5			Day 10		
G0/G1	70.5	74.3	71.5	67.2	67.0	68.3	72.2	75.0	73.9	71.2	71.1	68.6
S	14.6	14.1	13.9	14.9	14.5	13.2	14.2	10.6	13.8	11.6	13.4	14.8
G2/M	15.0	11.6	14.6	18.0	18.6	18.5	13.5	14.4	12.3	17.1	15.5	16.6

	RGD-PPCN						A5G81-PPCN					
	Day 5			Day 10			Day 5			Day 10		
G0/G1	74.2	75.6	74.4	61.8	62.4	66.0	60.2	60.0	59.1	55.1	55.2	54.6
S	13.1	11.3	13.4	21.1	22.8	17.3	21.0	19.6	20.9	26.6	24.0	25.9
G2/M	12.7	13.1	12.3	17.2	14.8	16.7	18.8	20.4	20.0	18.3	20.8	19.5

Table s1 | Cell cycle analysis data for the HDFs growing in Peptide-PPCN (data for Figure 4b)**.**

Fig. s8

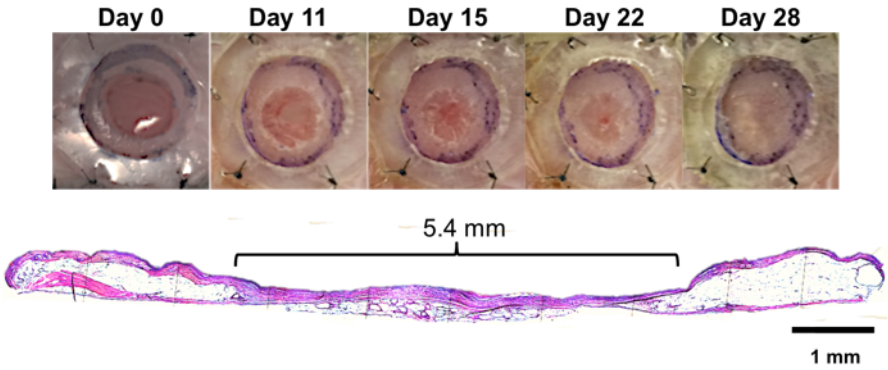

Figure s8 | The splints successfully limit wound contraction. Top: Digital pictures of a PBS-treated diabetic wound over time. The blue mark, which denotes the margin of the splint, remained in place throughout 28 days, confirming the successful splinting of the wound. Bottom: H&E staining image of the wound cross-section at day 30. The length of the regenerated granulation tissue is approximately 5.4 mm, which is comparable to the diameter of the initial wound (6 mm).

Fig. s9

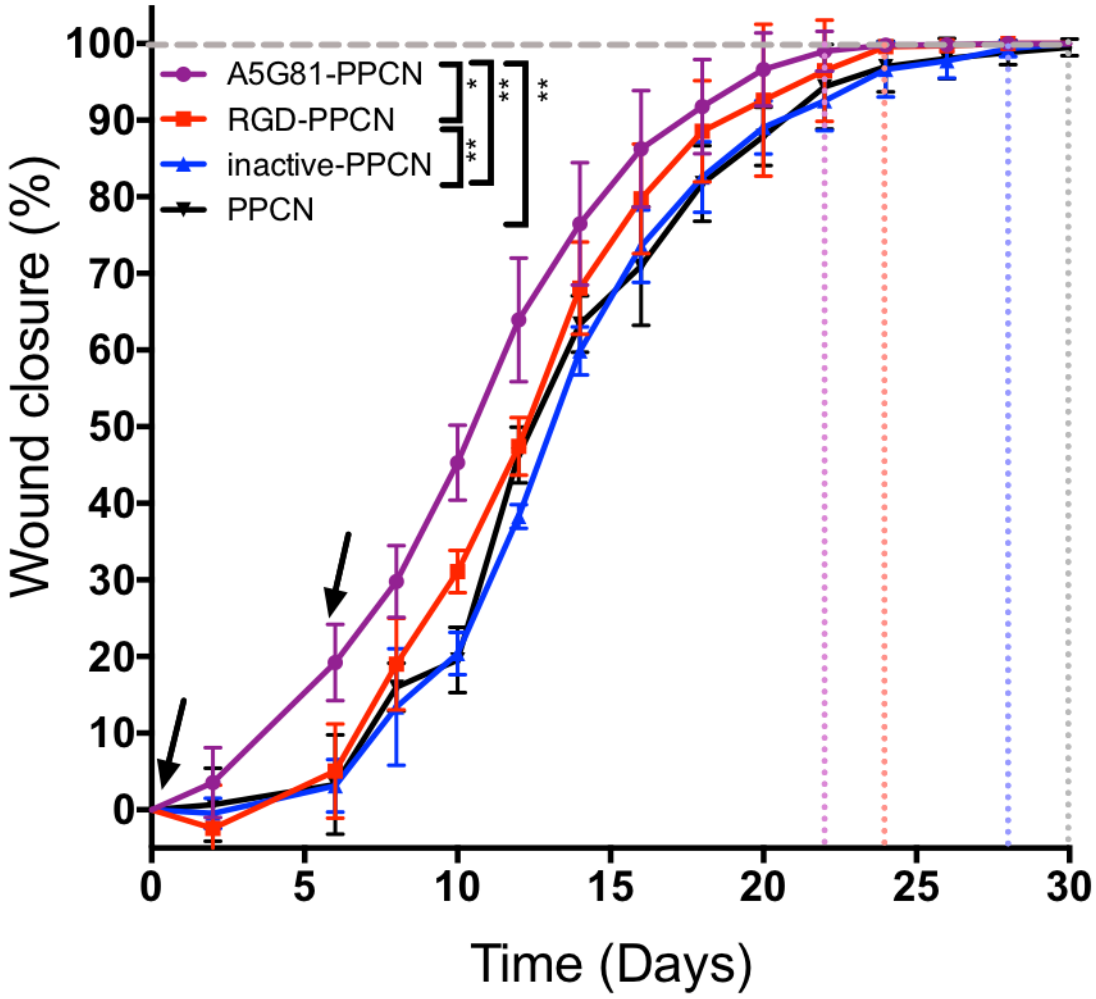

Figure s9 | A5G81-PPCN promotes accelerated regenerative wound closure of excisional splinted wounds in diabetic db/db mice. Quantification of complete wound closure over the course of 30 days for all four groups. All data are presented as mean ± SD. ($n \geq 5$; *$p<0.05$, **$p < 0.01$)

Fig. s10

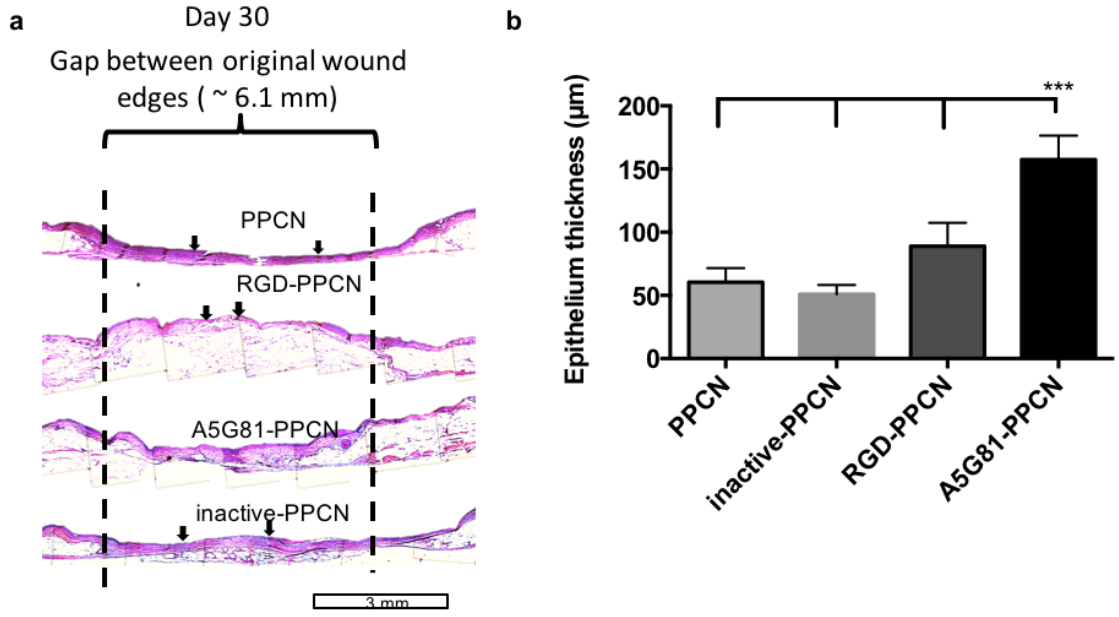

Figure s10 | Treatment of wounds with A5G81-PPCN enhances re-epithelialization at day 30. (a) Representative images of H&E tissue sections at day 30. Black dashed lines indicate the original wound edges; black arrowheads indicate the tips of the healing epithelial tongue (Scale bar: 3 mm). Compared to the initial wound size (6 mm), minimum wound contraction was observed in all four groups. **(b)** The epithelial layer at the center part of the wound was significantly thicker in the A5G81-PPCN-treated wounds at day 30. All data are presented as mean ± SD. ($n \geq 20$; *** $p < 0.001$)

Fig. s11

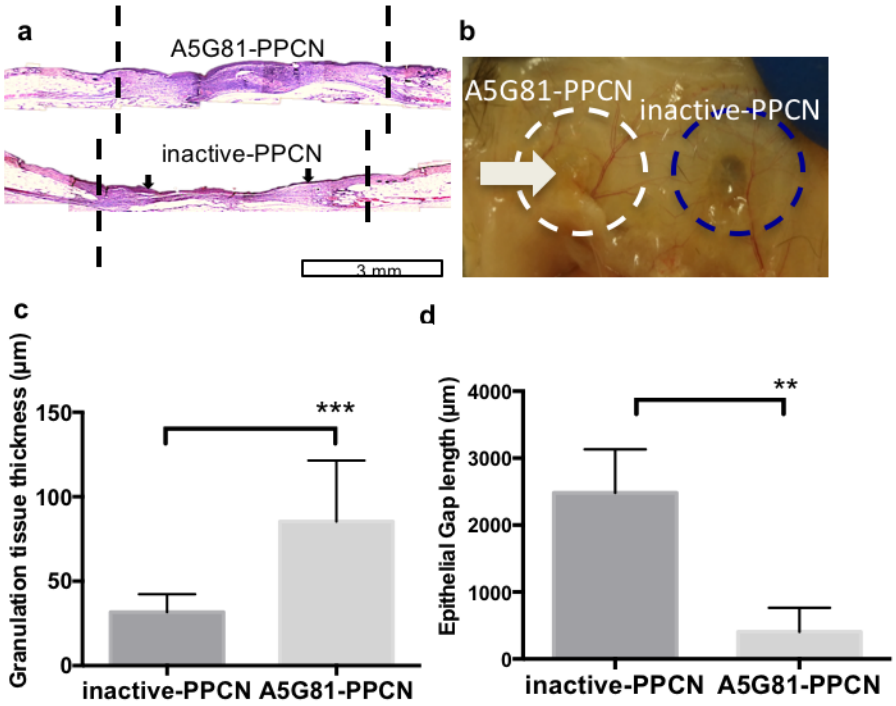

Figure s11 | A5G81-PPCN promotes enhanced re-epithelialization and granulation tissue formation at day 15. (a) Representative images of H&E tissue sections. Black dashed lines indicate wound edges; black arrowheads indicate the tips of the healing epithelial tongue (Scale bar: 3 mm). **(b)** Digital image of the bottom side of dermal tissue wounds of the same animal. Left: A5G81-PPCN; Right: inactive-PPCN. **(c)** Granulation tissue is thicker in the A5G81-PPCN-treated wounds. **(d)** Quantification of the epithelial gap shows a smaller gap and better closure in the A5G81-PPCN group. ($n \geq 20$; ** $p < 0.01$, *** $p < 0.001$)

Table s2. A brief summary of the published studies on laminin-derived peptides

Peptide sequence/name	Origin	Biological function	Application/animal model	Splinted wound (yes or not)	Tested in diabetes (yes or no)	Reported effect	Reference	Receptors involved
IKVAV	laminin α1	angiogenesis	peptide coated chitosan hydrogel/ mouse full thickness wound model	no	no	enhanced angiogenesis at the injection site	(1)	
RQVFQVAYIIIKA (A-13) & KAFDITYVRLKF (C-16)	laminin α1 & γ1	angiogenesis, reepit helialisation, granulation tissue	liquid application/ rat full thickness cutaneous wound model	no	no	accelerated reepithelialisation and granulation formation at early time points (4 days) no significance at a later (7 days) time points	(2)	αvβ3, α5β1
KKLRIKSKEK	laminin α3	epithelial attachment and migration, anti-inflammation and anti-granulation tissue formation	liquid application/ porcine partial-thickness cutaneous wounds model	no	no	promoted early-stage wound healing (day 4) by accelerating re-epithelialization	(3)	
KIPKPSSVPTELS AISML	laminin α3	keratinocytes migration	liquid application/ mouse full-thickness cutaneous wound model and a rabbit earlobe model	no	no	enhanced reepithelialisation (on day 8)	(4)	integrin β1
PPFLMLLKGSTR	laminin α3	reepithelialisation	peptide-coated chitin microfibrous matrices / rat full-thickness non-splinted wound model and rabbit earlobe model	no	no	promoted early-stage wound healing by accelerating re-epithelialization	(5)	α3β1
RKRLQVQLSIRT	laminin α1	keratinocytes attachment	peptide-modified chitosan membrane/ in vivo keratinocytes delivery in a nude mouse model	no	no	Delivered keratinocytes was able to established a stratified epidermis-like structure on the fascia	(6)	
AGQWHRVSVRW GC (A5G81)	laminin α5	dermal fibroblasts attachment and proliferation, keratinocytes attachment and migration, reepitheli alisation, granulation tissue formation	peptide modified antioxidant hydrogel/ mouse type II diabetic chronic full-thickness wound model	yes	yes	accelerated reepithelialisation and granulation formation throughout the entire course, reduced inflammation and oxidation induced DNA damage	this study	α3β1, α6β1

Fig. s12

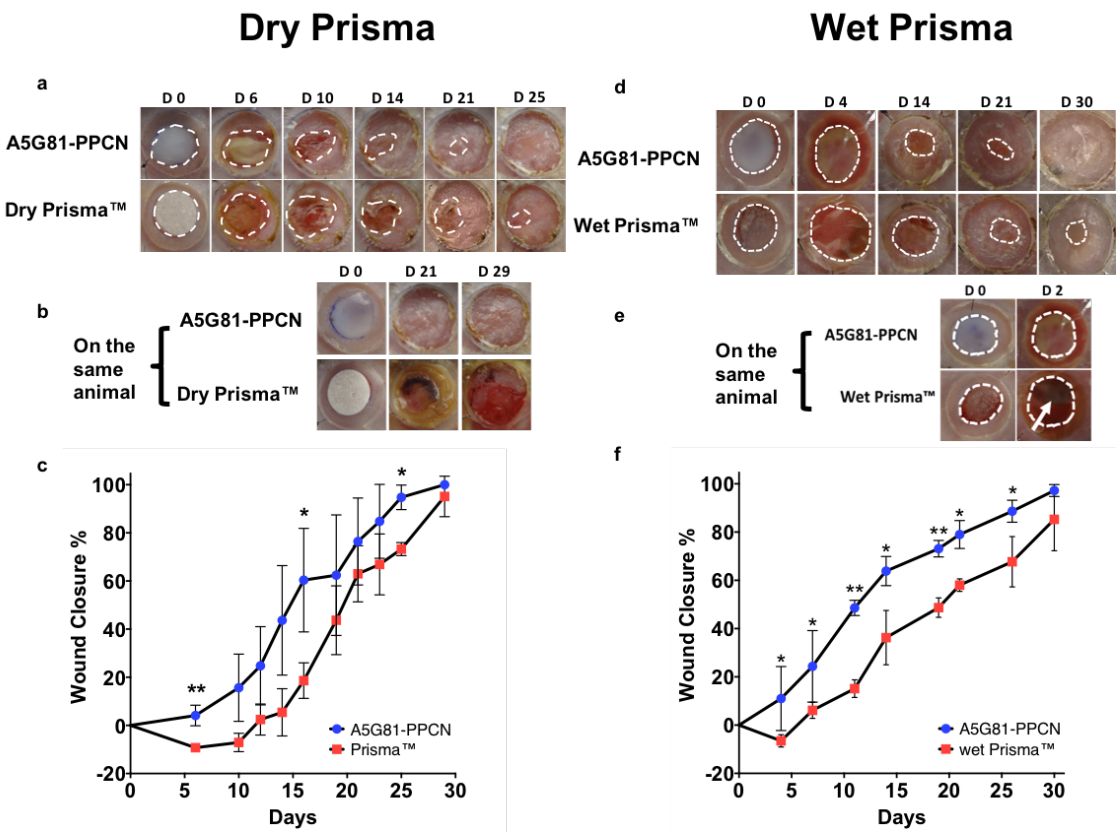

Figure s12 | A5G81-PPCN outperformed Promogran Prisma™ under both dry and wet conditions at enhancing the initial healing response of diabetic wounds. Left panel (dry Prisma^{TM}): **(a)** Representative images of the wound area during the course of healing. **(b)** Digital images of the two wounds on the same animal. During the study, one out of four wounds treated with the Prisma^{TM} matrix failed to heal within the 30-day time frame, while the wound on the contralateral side treated with A5G81-PPCN achieved complete closure by day 25. **(c)** Quantification of wound closure over the course of 29 days for A5G81-PPCN- and Prisma^{TM}-treated wounds. Right panel (wet Prisma^{TM}): **(d)** Representative images of the wound area during the course of healing. **(e)** Digital images of the two wounds on the same animal. The pre-swollen wet Prisma^{TM} matrix got shifted to the side of the wound one day after the surgery while A5G81-PPCN maintained its coverage. **(f)** Quantification of wound closure over the course of 30 days for A5G81-PPCN- and pre-swollen wet Prisma^{TM}-treated wounds. (n=3, * $p< 0.05$, ** $p< 0.01$)

Fig. s13

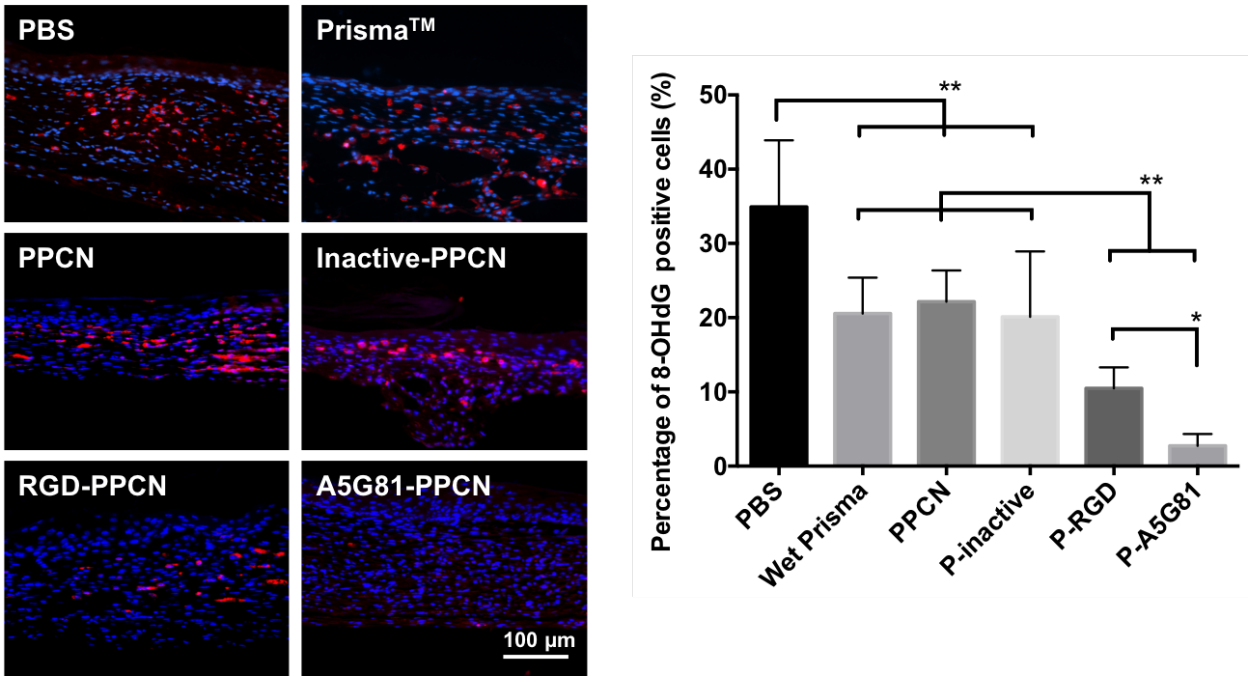

Figure s13 | Oxidative stressed-induced DNA damage was attenuated by the A5G81-PPCN treatment. (a) Representative images of the anti-8-OHdG antibody staining of the center part of the wound sections. **(b)** Quantification of the percentage of 8-OHdG positive cells for all 6 treatments. (n=6, * $p < 0.05$; ** $p < 0.01$)

Supplementary methods:

Materials and Methods

Peptide Synthesis and Characterization

Cysteine-terminated peptides were synthesized manually with Fmoc-Rink amide MHBA resin using the standard solid phase peptide synthesis protocol. After synthesis, the peptides were purified using reverse-phase high-performance liquid chromatography (HPLC) with a C18 column (Thermo Scientific, Waltham, MA). The final products were verified by their mass with matrix-assisted laser desorption/ionization time of flight mass spectrometry (MALDI-TOF MS).

PPCN Synthesis

PPCN was synthesized as described previously.(7) Briefly, we first synthesized the poly(polyethyleneglycol citrate) acrylate prepolymer (PPCac) by a polycondensation reaction at 140°C for 45 min under constant stirring at 300 rpm. The resulting solution was cooled to room temperature. Then, N-isoproylacrylamide monomer (NIPAM) was added to the PPCac prepolymer at a 1:1 w/w ratio and dissolved in 1,4-dioxane. The free radical initiator 2,2-azobisisobutyronitrile (AIBN) was added to the system after both PPCac and NIPAM were fully dissolved. Free radical polymerization was allowed to proceed for 8 hours at 65°C under nitrogen. The resulting PPCN copolymer was dissolved in 1,4-dioxane, purified by precipitation in diethyl ether and vacuum-dried.

Determination of the Lower Critical Solution Temperature

The lower critical solution temperatures of the PPCN and PPCN-peptide hydrogels were determined using a Discovery Hybrid Rheometer (TA Instruments, DE). The storage and loss moduli of the gels were measured at a frequency of 1 Hz and a heating rate of 1°C/min from 15 °C to 35 °C, using a 2% amplitude and a 6 s^{-1}angular frequency. The LCST was defined by the crossing point of the loss and storage modulus curves.

Antioxidant Activity Assessment

The antioxidant activity of the PPCN-peptide hydrogels was determined using the β-carotene-linoleic acid assay as previously described by us.(7)

In Vitro 3D Cell Culture

Human epithelial keratinocytes (HEKa) or human dermal fibroblasts (HDF) were mixed with cold PPCN-peptide solutions (100K cells/mL gel), added to wells of uncoated μ-slides (ibidi, Madison, WI) and allowed to gel at 37°C for 1-2 min. Cell culture medium (KGM-Gold for HEKa, DMEM+10%FBS for HDF) was then added to each well, and cells were cultured at 37°C in 5% CO_2. After 5 or 10 days, the gels were washed twice with warm PBS, and stained with 2 uM calcein AM and 2 uM ethidium homodimer-1 at 37°C for 15 min to identify live and dead cells. The samples were then washed twice with warm 1X PBS and imaged on a Nikon C2 Confocal Microscope.

SAM Surface Preparation

SAM surfaces were prepared as previously described.(8) Briefly, glass coverslips were first coated with 2 nm Ti, followed by 11 nm Au using an electron beam evaporator. The gold-coated surfaces were then soaked overnight at 4°C in an ethanolic solution of 98%

symmetric tri(ethylene glycol)-terminated dioctadecyl disulfide and 2% asymmetric maleimide and tri(ethylene glycol)-terminated dioctadecyl disulfide to obtain a mixture of 1% maleimide and 99% tri(ethylene glycol). Before use, the prepared SAM coverslips were rinsed with ethanol, water, ethanol once again, dried under a nitrogen stream, and cut into approximately 1x1 cm pieces for use in cell culture experiments.

Cell Adhesion on Peptide-presenting SAM Surface

The synthesized peptides were immobilized onto SAM chips by incubating the slides with 100 μM peptide solution in PBS at room temperature for 1 hr. The peptide slides were then rinsed three times with PBS, and cells were immediately seeded on the surfaces at a density of 20,000 cells/cm^2. Cells were incubated at 37°C in 5% CO_2 for 1 hr to allow cell attachment. The surfaces were then rinsed with PBS and the adherent cells were fixed in 4% paraformaldehyde. Peptide chips were then mounted with Vectashield + DAPI and imaged on a Nikon Eclipse TE2000-U inverted fluorescence microscope. The number of cells per field of view was counted using ImageJ software (NIH, Bethesda, MD). The cell number per area for each chip was based on the average of 5 fields of view.

Cell Migration on Peptide-presenting SAM Surface

HEKa cells were seeded at a density of 10,000 cells/cm^2 on the 1% peptide SAM surfaces. The cells were allowed to adhere to the surface for 2 h at 37 °C in 5% CO_2, and after 2 h, the surfaces were then rinsed with PBS to remove the non-adherent cells. The cell migration path on the cell-seeded SAM surfaces was tracked using a live-cell imaging chamber (ibidi) and the Leica Spinning Disk AF system (Leica, Wetzlar, Germany). Images were acquired at nine places on each chip through a 10x objective every 2 min for 2 h. The cell migration was then quantified using ImageJ (NIH) software.

Global Gene Expression Analysis

The RNA of the HEKas cultured on A5G81-SAM and the control RGD-SAM surfaces was extracted using Ambion RNAqueous kit (Thermo Fisher) according to the manufacture's protocol. RNA sample quality was checked by Agilent 2100 Bioanalyzer by the Next Generation Sequencing Core at Northwestern University. RNA expression profiling was performed in triplicates using the Single-end, 75bp, high-output runs. Raw data processing and identification of differentially expressed genes was performed by the Bioinformatics Core at Northwestern University. Differentially expressed genes were identified using an Analysis of Variance (ANOVA) model with empirical Bayesian variance estimation on the basis of a statistically significant (adjusted p value <0.05) and $2^{0.5}$ absolute fold change in expression level. Genes functional analysis and process clustering were performed using GOrilla search for enriched GO terms (process and pathway analysis), with FDR< 0.05.(9)

Cell Proliferation Quantification

HDFs were entrapped in the hydrogel scaffold samples and cultured using the same method as the *in vitro* 3D cell culture studies using 10,000 cells per 50 μl hydrogel per sample. At each time point, after removing the medium, the samples were cooled on ice, and the cells were lysed by PBS-3% Triton-X. The Quant-iT PicoGreen dsDNA assay kit (Life Technologies) was employed according to the manufacturer's protocol,

and the results were read in triplicates. Samples of 100 mL were assessed using microplate reader (Tecan, Männedorf, Switzerland). Fluorescence was quantified at 520 nm with excitation at 480 nm.

Cell Cycle Analysis

Flow cytometry with propidium iodide (PI), was performed in order to measure the cell cycle activity. At each time point, hydrogels containing cells were liquefied by cooling, and cells were isolated via centrifugation. The cells were then washed with ice-cold PBS, and fixed with 70% ice-cold ethanol for 1 h before repeated washing with PBS and re-suspension in PBS with 0.5 mg/mL Rnase A (Thermo Fisher Scientific). After 1 h incubation, the cellular DNA was then stained with PI (50 µg/mL) for 20 min in the dark at 4 °C. The relative DNA concentration of the stained cells was measured using a BD LSRII flow cytometer (Becton Dickinson, San Jose, CA).

Assessment of Cell Proliferation Inhibition

The mouse monoclonal antibody against human integrin α6 and α3 were purchased from Santa Cruz (Dallas, TA), and dialyzed with 10,000 MWCO Dialysis Cassettes dialysis cassette (Thermo Fisher, PA) overnight to remove the sodium azide. For the proliferation inhibition study, P-A5G81 and PPCN hydrogel scaffolds were prepared as 100 mg/ml PBS solution as described above. Before cell encapsulation, HDFs were pre-incubated in suspension with corresponding anti-integrin antibodies (final concentration 10 µg/ mL) for 15 min at 37°C. Then the pre-treated HDFs ($1x10^4$ cells per 50 µL scaffold per well) were incubated on the ultra-low attachment plate (Coring, Coring, NY) for 5 days at 37°C in 5% CO_2. Anti-integrin antibodies treatments were also added in the culture media for the corresponding groups (10 µg/ mL), and the media was changed every other day. After 5 days of incubation, total DNA content within each scaffold was quantified using PicoGreen DNA quantification assay as mentioned above.

Diabetic Wound Healing Model

The *in vivo* performance of the hydrogels was evaluated using a splinted excisional wound model in db/db mice (BKS.Cg-Dock7^{m} +/+ Lepr^{db}/J Homozygous for Lepr^{db}) as previously described and according to the approval of Northwestern University's institutional animal care and use committee.(10-12) The animals were separated into 3 groups of five animals, with each group receiving one of the following treatments: (1) A5G81-PPCN vs. PRGD-PCN, (2) A5G81-PPCN vs. inactive-PPCN, or (3) A5G81-PPCN vs. PPCN. To prevent skin contraction, paired sterilized doughnut-shaped acrylate splints (10-mm inner diameter; 12-mm outer diameter) (3M, St. Paul, MN) were attached to the left and right dorsal sides of the mouse with Vetbond (3M) and interrupted 6-0 nylon sutures (Ethicon, Cincinnati, OH) after depilation. A 6-mm circular, full-thickness wound was made in the center of each splinted area. 40 µl of gel solution was applied to each wound bed. A transparent sterile occlusive dressing TegaDerm™ (3M) was then placed over the wound and the splint. Digital images of the wound area were taken every other day and quantified by three blinded observers using ImageJ by normalizing the wound area to the known splint area at each time point. Hydrogel dressings were reapplied on day 6, after gently rinsing the wound with cold PBS. To benchmark A5G81-PPCN against a clinically used wound dressing, an additional set of

four animals received A5G81-PPCN in one wound and Promogran Prisma™ matrix wound dressing (Systagenix, Gatwick, UK) in the contralateral wound.

Tissue Processing and Histology

Upon full closure of the wounds (for the first study) or 10 days after creating the wound (for the second study), animals were euthanized, and the regenerated wound tissue was excised with a 10-mm biopsy punch (Acuderm, Fort Lauderdale, FL), fixed using 4% paraformaldehyde and embedded by paraffin. The tissues were then sectioned and stained with hematoxylin and eosin (H&E) to measure granulation tissue thickness and the epithelial gap via histomorphometry. The granulation tissue was quantified by measuring the thickness at 5 evenly spaced locations from the center of the wound for each animal using ImageJ. The average of the measurements obtained from each wound was calculated and compared among treatment groups using one-way ANOVA Tukey multiple comparison test. Epithelial gap and epithelial thickness were quantified based on images taken at the center of the wound for each treatment group. The tissue sections were also stained for Keratin 10, Integrin α3 or F4/80 (Santa Cruz, Dallas, TX). The secondary antibodies used were either conjugated to AlexaFluor488 or AlexaFluor555 (Invitrogen, Carlsbad, CA). Controls consisted of samples stained with the secondary antibody without incubation with a primary antibody.

Reference:

1. Kibbey MC, Grant DS, & Kleinman HK (1992) Role of the SIKVAV site of laminin in promotion of angiogenesis and tumor growth: an in vivo Matrigel model. *Journal of the National Cancer Institute* 84(21):1633-1638.
2. Malinda KM, Wysocki AB, Koblinski JE, Kleinman HK, & Ponce ML (2008) Angiogenic laminin-derived peptides stimulate wound healing. *The international journal of biochemistry & cell biology* 40(12):2771-2780.
3. Rousselle P*, et al.* (2013) The syndecan binding sequence KKLRIKSKEK in laminin alpha3 LG4 domain promotes epidermal repair. *European journal of dermatology : EJD*.
4. Araki E*, et al.* (2009) Clustering of syndecan-4 and integrin beta1 by laminin alpha 3 chain-derived peptide promotes keratinocyte migration. *Molecular biology of the cell* 20(13):3012-3024.
5. Min SK*, et al.* (2010) The effect of a laminin-5-derived peptide coated onto chitin microfibers on re-epithelialization in early-stage wound healing. *Biomaterials* 31(17):4725-4730.
6. Ikemoto S*, et al.* (2006) Laminin peptide‐conjugated chitosan membrane: Application for keratinocyte delivery in wounded skin. *Journal Of Biomedical Materials Research Part A* 79(3):716-722.
7. Yang J, Van Lith R, Baler K, Hoshi RA, & Ameer GA (2014) A thermoresponsive biodegradable polymer with intrinsic antioxidant properties. *Biomacromolecules* 15(11):3942-3952.

8. Sobers CJ, Wood SE, & Mrksich M (2015) A gene expression-based comparison of cell adhesion to extracellular matrix and RGD-terminated monolayers. *Biomaterials* 52(1):385--394.
9. Eden E, Navon R, Steinfeld I, Lipson D, & Yakhini Z (2009) GOrilla: a tool for discovery and visualization of enriched GO terms in ranked gene lists. *BMC Bioinformatics* 10(1):48.
10. Zhu Y*, et al.* (2016) Sustained release of stromal cell derived factor-1 from an antioxidant thermoresponsive hydrogel enhances dermal wound healing in diabetes. *Journal of Controlled Release* 238:114--122.
11. Galiano RD, Michaels Jt, Dobryansky M, Levine JP, & Gurtner GC (2004) Quantitative and reproducible murine model of excisional wound healing. *Wound Repair Regen* 12(4):485-492.
12. Michaels Jt*, et al.* (2007) db/db mice exhibit severe wound-healing impairments compared with other murine diabetic strains in a silicone-splinted excisional wound model. *Wound Repair Regen* 15(5):665-670.